

# Informed Hybrid Zonotope-based Motion Planning Algorithm

Peng Xie, Johannes Betz, Amr Alanwar

**Abstract**—Optimal path planning in nonconvex free spaces is notoriously challenging, as formulating such problems as mixed-integer linear programs (MILPs) is *NP-hard*. We propose HZ-MP, an *informed Hybrid Zonotope-based Motion Planner*, as an alternative approach that decomposes the obstacle-free space and performs low-dimensional face sampling guided by an ellipsotope heuristic, enabling focused exploration along promising transit regions. This structured exploration eliminates the excessive, unreachable sampling that degrades existing informed planners such as AIT\* and EIT\* in narrow gaps or boxed-goal scenarios. We prove that HZ-MP is *probabilistically complete* and *asymptotically optimal*. It converges to near-optimal trajectories in finite time and scales to high-dimensional cluttered scenes.

## I. INTRODUCTION

Motion planning in robotics requires finding collision-free paths through complex environments. Optimization-based methods formulate this as a mixed-integer program (MIP) to encode obstacle avoidance, but solving these programs is NP-hard and generally intractable for real-time use [1]. This allows for optimal trajectory generation under dynamic and kinematic constraints, but at a steep computational cost: solving the resulting mixed-integer linear or quadratic programs is NP-hard and generally intractable for real-time use on embedded hardware [1]. Recent advances have aimed to mitigate this complexity. For example, the hybrid zonotope representation of obstacle-free space has been introduced to compactly model nonconvex regions with a combination of continuous and binary variables [2]. By using hybrid zonotopes to encode obstacles within an MPC, one can tighten convex relaxations and exploit problem structure, yielding order-of-magnitude speed-ups in mixed-integer solver performance[3]. To address these computational challenges, recent works have developed multi-stage Mixed-Integer Quadratic Programming (MIQP) methods that replace direct non-convex computations with structured decompositions. These approaches employ custom Branch-and-Bound algorithms integrated with Interior-Point solvers, achieving significant speedups in the optimization process [3]. However, MIQP methods still face fundamental limitations in complex scenarios. Consider a vehicle that must optimize not only position and velocity but also acceleration, jerk, and load distribution—resulting in state spaces with

Peng Xie and Amr Alanwar are with the TUM School of Computation, Information and Technology, Department of Computer Engineering, Technical University of Munich, 74076 Heilbronn, Germany. (e-mail: p.xie@tum.de, alanwar@tum.de)

Johannes Betz is with the TUM School of Engineering and Design, Department of Mobility Systems Engineering, Technical University of Munich, 85748 Garching, Germany. (e-mail: johannes.betz@tum.de)

dozens of dimensions. In such high-dimensional settings, MIQP suffers from the curse of dimensionality: exponentially growing integer variables, massive constraint matrices, and dramatically increased solution times. Furthermore, the Branch-and-Bound algorithm provides little predictability—it may find solutions quickly or require exploring exponentially many branches, making it unsuitable for real-time guarantees[4]. These inherent limitations of optimization-based approaches motivate exploring alternative paradigms for efficient motion planning

Another class of motion planners relies on random sampling to explore the state space. Early algorithms such as the probabilistic roadmap (PRM) and rapidly-exploring random tree (RRT) families are *probabilistically complete* but not optimal by design [5], [6]. The *informed* variants bias samples toward cost-bounded ellipsoidal subsets to accelerate convergence; e.g. Informed RRT\* already improves on uniform RRT\* [7]. Notably, adaptively informed trees and effort informed trees employ an asymmetric bidirectional search where two growing trees continuously guide each other using updated cost-to-go estimates [8]. However, their stochastic exploration can stall in narrow-gap or double-enclosure scenarios where most samples fall in unreachable regions, slowing convergence to the global optimum.[8]

We propose HZ-MP (informed Hybrid Zonotope-based Motion Planner), which synergizes optimization-based and sampling-based planning through four key steps illustrated in Fig. 1:

(a)→(b) *Space decomposition*: We represent the obstacle-free space with hybrid zonotopes—finite collections of convex leaves with discrete transitions, transforming the complex non-convex environment into a structured representation amenable to systematic exploration.

(b)→(c) *Path identification*: We compute adjacency relationships between leaves and identify all possible connected paths. Our approach samples on  $(n - 1)$ -dimensional shared faces rather than  $n$ -dimensional volumes and performs parallel computation across all potential paths simultaneously to obtain the optimal solutions. In Fig. 1(c), three different colored paths represent possible routes, with the brown path identified as currently optimal.

(c)→(d) *Ellipsotope construction*: Using the current optimal path cost, we construct an ellipsotope reachable set that bounds all states potentially leading to improved solutions, as shown in Fig. 1(d).

(d)→(e) *Reachable set refinement*: We prune search regions using ellipsotope-based reachability bounds to update the feasible space, creating a refined reachable set for subsequent planning iterations, demonstrated in Fig. 1(e).

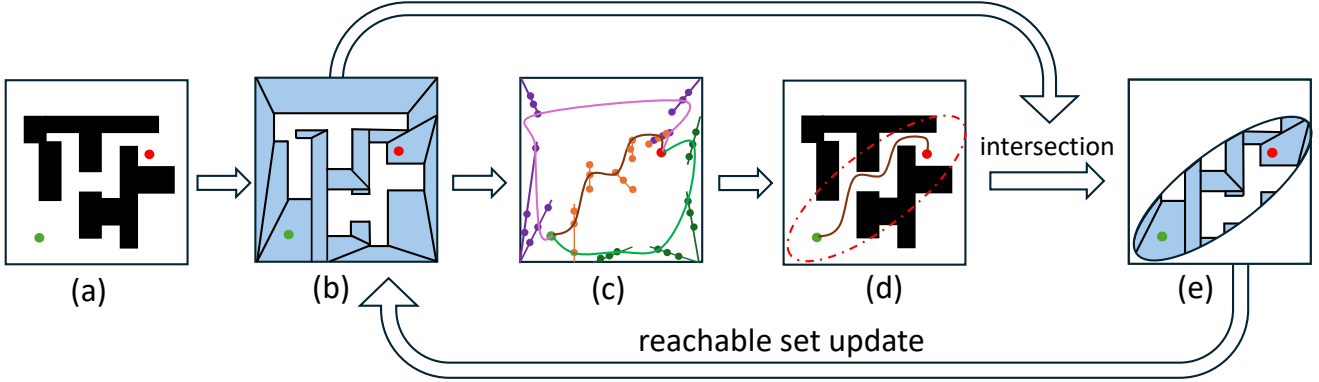


Fig. 1: Overview of HZ-MP process illustration. (a) Original environment with obstacles (black), start (green), and goal (red). (b) Hybrid zonotope representation of obstacle-free space decomposed into convex leaves. (c) Three possible connected paths identified through adjacency computation, with the brown path being the shortest. (d) Ellipsotope reachable set constructed based on the optimal path cost from (c). (e) Updated reachable set after pruning using ellipsotope-based bounds, which refines the feasible space for subsequent planning iterations.

This iterative process enables HZ-MP to efficiently balance global optimality with computational efficiency by systematically reducing the search space while maintaining solution completeness.

By combining these techniques, HZ-MP effectively balances the global optimality of MPC-based methods with the adaptivity and speed of informed sampling. The proposed planner is probabilistically complete and asymptotically optimal, while exhibiting significant practical speed-ups over existing approaches. Our method brings motion planning closer to achieving the high solution quality of optimization-based methods while operating within the strict timing constraints of real-time applications.

The remainder of this paper is organized as follows. Section II introduces mathematical preliminaries on hybrid zonotopes and ellipsotopes. Section III presents the HZ-MP algorithm with theoretical guarantees. Section IV demonstrates the algorithm's effectiveness through numerical examples. Section V concludes with future research directions.

## II. NOTATIONS AND PRELIMINARIES

This section introduces the mathematical foundations necessary and notations for our hybrid zonotope-based motion planning algorithm.

### A. Notations

Matrices are denoted by uppercase letters, e.g.,  $G \in \mathbb{R}^{n \times n_g}$ , and sets by uppercase calligraphic letters, e.g.,  $\mathcal{Z} \subset \mathbb{R}^n$ . Vectors and scalars are denoted by lowercase letters, e.g.,  $b \in \mathbb{R}^{n_c}$ . The  $n$ -dimensional unit hypercube is denoted by  $\mathcal{B}_\infty^n = \{x \in \mathbb{R}^n \mid \|x\|_\infty \leq 1\}$ . The set of all  $n$ -dimensional binary vectors is denoted by  $\{-1, 1\}^n$ . The cardinality of the discrete set  $\mathcal{T}$  is denoted by  $|\mathcal{T}|$ , e.g.,  $|\mathcal{T}| = 8$  for  $\mathcal{T} = \{-1, 1\}^3$ . The concatenation of two column vectors into a single column vector is denoted by  $(\xi_1 \ \xi_2) = [\xi_1^T \ \xi_2^T]^T$ . The bold  $\mathbf{1}$  and  $\mathbf{0}$  denote matrices of all 1 and 0 elements, respectively, and  $\mathbf{I}$  denotes the

identity matrix with dimensions indicated by subscripts when not easily deduced from context. Given the sets  $\mathcal{Z}, \mathcal{W} \subset \mathbb{R}^n$ ,  $\mathcal{Y} \subset \mathbb{R}^m$ , and matrix  $R \in \mathbb{R}^{m \times n}$ , the linear mapping of  $\mathcal{Z}$  by  $R$  is  $R\mathcal{Z} = \{Rz \mid z \in \mathcal{Z}\}$ , the Minkowski sum of  $\mathcal{Z}$  and  $\mathcal{W}$  is  $\mathcal{Z} \oplus \mathcal{W} = \{z + w \mid z \in \mathcal{Z}, w \in \mathcal{W}\}$ , the generalized intersection of  $\mathcal{Z}$  and  $\mathcal{Y}$  under  $R$  is  $\mathcal{Z} \cap_R \mathcal{Y} = \{z \in \mathcal{Z} \mid Rz \in \mathcal{Y}\}$ , and the union of  $\mathcal{Z}$  and  $\mathcal{W}$  is  $\mathcal{Z} \cup \mathcal{W} = \{x \in \mathbb{R}^n \mid x \in \mathcal{Z} \vee x \in \mathcal{W}\}$ .

### B. Hybrid zonotope

Hybrid zonotopes provide a powerful representation for nonconvex sets by combining continuous and binary factors. Each combination of binary factors defines a constrained zonotope, which we call a leaf of the hybrid zonotope. Understanding the adjacency relationships between these leaves is crucial for applications such as motion planning and reachability analysis. We start by defining the hybrid zonotope set representation.

**Definition II.1** ([2]). The set  $\mathcal{Z}_h \subset \mathbb{R}^n$  is a hybrid zonotope if there exist  $G^c \in \mathbb{R}^{n \times n_g}$ ,  $G^b \in \mathbb{R}^{n \times n_b}$ ,  $c \in \mathbb{R}^n$ ,  $A^c \in \mathbb{R}^{n_c \times n_g}$ ,  $A^b \in \mathbb{R}^{n_c \times n_b}$ , and  $b \in \mathbb{R}^{n_c}$  such that

$$\mathcal{Z}_h = \left\{ [G^c \ G^b] \begin{bmatrix} \xi^c \\ \xi^b \end{bmatrix} + c \begin{cases} \begin{bmatrix} \xi^c \\ \xi^b \end{bmatrix} \in \mathcal{B}_\infty^{n_g} \times \{-1, 1\}^{n_b}, \\ [A^c \ A^b] \begin{bmatrix} \xi^c \\ \xi^b \end{bmatrix} = b \end{cases} \right\}. \quad (1)$$

Central to our approach is the decomposition of complex obstacle-free environments into manageable convex regions, each represented as a leaf of a hybrid zonotope.

**Example 1.** We can represent the map with obstacles shown in Figure 2 using a hybrid zonotope. Consider the blue region with an obstacle (white area) in the center. This non-convex feasible space is captured by:

$$\mathcal{HZ} = \langle G_c, G_b, c, A_c, A_b, b \rangle \quad (2)$$

where  $c = [-41.25, 2.5]^T \in \mathbb{R}^2$  is the center,  $G_c \in \mathbb{R}^{2 \times 28}$  contains the continuous generators, and  $G_b = \mathcal{O}_{2 \times 4}$  (indicat-

ing all binary modes share the same center). The constraint matrices  $A_c \in \mathbb{R}^{16 \times 28}$ ,  $A_b \in \mathbb{R}^{16 \times 4}$ , and  $b \in \mathbb{R}^{16}$  encode the logical constraints that exclude the obstacle region.

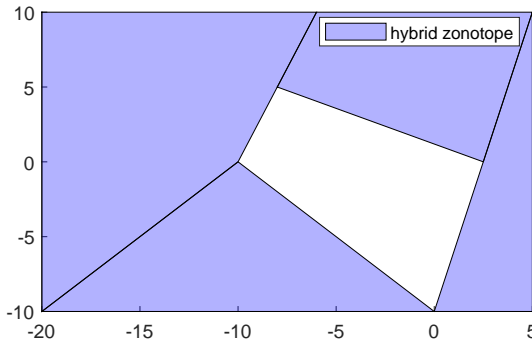


Fig. 2: A hybrid zonotope representation of a non-convex feasible region with an obstacle (white area).

### C. Informed sampling

The optimal path planning problem seeks to find a valid path  $\sigma^*$  from a start state  $x_{\text{start}}$  to a goal region  $X_{\text{goal}}$  that minimizes a cost function  $c(\sigma)$  [6]. Sampling-based planning algorithms are considered almost-surely asymptotically optimal if, as the number of samples approaches infinity, they find a solution whose cost converges to the optimal cost with probability 1.

Informed sampling techniques enhance the performance of these algorithms by focusing the sampling process on regions more likely to contain high-quality solutions. Informed RRT\* [7] exemplifies this approach by restricting sampling to an ellipsoidal subset of the state space once an initial solution is found. This informed subset, defined as

$$X_{\text{informed}} = \{x \in X \mid \|x_{\text{start}} - x\| + \|x - x_{\text{goal}}\| \leq c_{\text{best}}\}, \quad (3)$$

contains all states that could potentially improve the current best solution with cost  $c_{\text{best}}$ .

A significant theoretical advantage of informed sampling is its convergence rate:

**Theorem II.2** ([7]). *With uniform sampling of the informed subset,  $x \sim \text{Uniform}(X_{\text{informed}})$ , the cost of the best solution,  $c_{\text{best}}$ , converges linearly to the theoretical minimum,  $c_{\min}$ , in the absence of obstacles.*

This linear convergence rate offers substantial improvements over the sublinear convergence of uniform sampling across the entire state space. Recent advances in bidirectional informed sampling techniques [8] further build upon this foundation to achieve even more efficient path planning.

### D. Ellipsoids and ellipsotopes

To represent the informed region described above, we employ ellipsotopes, which generalize ellipsoids and provide an efficient framework for capturing feasible subsets of the state space.

**Definition II.3** (Ellipsoids and Ellipsotopes [9]). An ellipsoid is the set

$$\mathcal{E}(c, Q) = \{x \in \mathbb{R}^n \mid (x - c)^\top Q(x - c) \leq 1\}, \quad (4)$$

where  $c \in \mathbb{R}^n$  is the center and  $Q \succ 0$  is a positive definite shape matrix. Generalizing the ellipsoid concept, an ellipsotope is a set

$$\mathcal{E}_p(c, G, A, b, \mathcal{I}) = \{c + G\xi \mid \|\xi_J\|_p \leq 1 \forall J \in \mathcal{I} \text{ and } A\xi = b\} \subset \mathbb{R}^n, \quad (5)$$

where  $c \in \mathbb{R}^n$ ,  $G \in \mathbb{R}^{n \times n_g}$ ,  $A \in \mathbb{R}^{n_c \times n_g}$ ,  $b \in \mathbb{R}^{n_c}$ , and  $\mathcal{I}$  is a valid index set.

## III. INFORMED HYBRID ZONOTOPE-BASED MOTION PLANNING WITH SPACE DECOMPOSITION

### A. Problem Formulation and Overview

Consider the optimal motion planning problem: Given a start state  $x_{\text{start}} \in \mathcal{X}_{\text{free}}$  and goal state  $x_{\text{goal}} \in \mathcal{X}_{\text{free}}$ , find a continuous collision-free path  $\sigma : [0, 1] \rightarrow \mathcal{X}_{\text{free}}$  that minimizes a cost function:

$$\sigma^* = \arg \min_{\sigma} c(\sigma), \quad \text{s.t. } \sigma(0) = x_{\text{start}}, \sigma(1) = x_{\text{goal}} \quad (6)$$

Our HZ-MP approach addresses this problem through the systematic process illustrated in Figure 1. The algorithm transforms the complex non-convex planning problem into a structured exploration of convex regions, enabling efficient path optimization while maintaining completeness guarantees. We now detail each component of this process.

### B. Free space decomposition via hybrid zonotopes

The first step in our approach, illustrated in Figure 1(a)-(b), transforms the obstacle-laden environment into a structured representation amenable to efficient exploration. Given a state space  $\mathcal{X} \subset \mathbb{R}^n$  with obstacles  $\mathcal{X}_{\text{obs}}$ , we decompose the free space  $\mathcal{X}_{\text{free}} = \mathcal{X} \setminus \mathcal{X}_{\text{obs}}$  into hybrid zonotopes.

- *Nef polyhedron representation:* We employ CGAL's Nef polyhedron framework to compute  $\mathcal{X}_{\text{free}} = \mathcal{X} \setminus \mathcal{X}_{\text{obs}}$  through exact Boolean operations. This approach guarantees topologically consistent results even for complex non-manifold geometries with holes or narrow passages, while preserving the face-edge incidence relationships essential for adjacency computation [10].
- *Convex decomposition:* The resulting Nef polyhedron is partitioned into convex components  $\{C_1, C_2, \dots, C_m\}$  such that  $\mathcal{X}_{\text{free}} = \bigcup_{i=1}^m C_i$ , yielding a finite collection of convex regions suitable for hybrid zonotope construction [11].

The resulting decomposition is represented by a vertex matrix  $V = [\mathbf{v}_1, \dots, \mathbf{v}_{n_v}] \in \mathbb{R}^{n \times n_v}$  containing all vertices of the convex components, and an incidence matrix  $M \in \mathbb{R}^{n_v \times n_F}$  [12]. From this V-representation, we construct a hybrid zonotope using the methodology in [13], which enables efficient conversion from V-rep polytopes to a unified hybrid zonotope. This transformation preserves the topology of the free space while providing a representation amenable to sampling-based motion planning algorithms.

The hybrid zonotope representation provides a finite collection of convex regions  $\mathcal{L} = \{\mathcal{Z}_1, \dots, \mathcal{Z}_m\}$ , transforming the continuous planning problem into a discrete graph search augmented with continuous optimization within each region. To leverage this structure, we next establish connectivity relationships between these regions.

### C. Adjacency computation and path identification

Having decomposed the free space into convex leaves as shown in Figure 1(b), we must establish connectivity relationships to identify feasible paths. This adjacency information, visualized in Figure 1(c) forms the foundation for our dimension-reduced sampling strategy.

When representing obstacle-free environments using hybrid zonotopes, the complex non-convex space decomposes into simpler convex regions called "leaves," each corresponding to a specific configuration of binary variables. The critical insight for path planning is identifying which regions are adjacent—sharing boundaries where paths can transition smoothly between them. This adjacency information creates a structured roadmap for navigation, enabling focused sampling on region boundaries rather than uniform space exploration and guaranteeing collision-free paths within each convex region.

*Remark III.1.* Given a hybrid zonotope  $\mathcal{Z}_h = \langle G^c, G^b, c, A^c, A^b, b \rangle$  as defined in Definition II.1, we can decompose it into a collection of constrained zonotopes and establish their connectivity through the following:

- (i) Based on [2, Theorem 5], let  $\xi_i^b$  be an entry of the discrete set  $\{-1, 1\}^{n_b}$  containing  $2^{n_b}$  elements. The feasible entries  $\mathcal{L}$  is defined as:

$$\mathcal{L} = \{\xi_i^b \in \{-1, 1\}^{n_b} \mid \exists \xi^c \in \mathcal{B}_{\infty}^{n_g} \text{ s.t. } A^c \xi^c + A^b \xi_i^b = b\} \quad (7)$$

- (ii) For each  $\xi_i^b \in \mathcal{L}$ , the corresponding constrained zonotope is defined as:

$$\mathcal{Z}_{c,i} = \langle G^c, c + G^b \xi_i^b, A^c, b - A^b \xi_i^b \rangle \quad (8)$$

- (iii) An indexing function  $\text{ID} : \mathcal{L} \rightarrow \{1, 2, \dots, |\mathcal{L}|\}$  assigns a unique integer to each leaf, allowing us to define the adjacency matrix  $\mathcal{A} \in \{0, 1\}^{|\mathcal{L}| \times |\mathcal{L}|}$  as:

$$\mathcal{A}_{ij} = \begin{cases} 1 & \text{if } \mathcal{Z}_{c,i} \cap \mathcal{Z}_{c,j} \neq \emptyset \\ 0 & \text{otherwise} \end{cases} \quad (9)$$

where  $i = \text{ID}(\xi_i^b)$  and  $j = \text{ID}(\xi_j^b)$  for  $\xi_i^b, \xi_j^b \in \mathcal{L}$ .

This decomposition and adjacency structure provide a complete topological representation of the hybrid zonotope that can be systematically explored for motion planning applications.

**Proposition III.2.** Let  $\mathcal{Z}_h = \langle G^c, G^b, c, A^c, A^b, b \rangle$  be a hybrid zonotope with leaves  $\mathcal{Z}_{c,i}, \mathcal{Z}_{c,j}$  from (8). Define,

$$M = \begin{bmatrix} G^c \\ A^c \end{bmatrix}, N = \begin{bmatrix} G^b \\ A^b \end{bmatrix}, \xi^c = \xi_i^c, \quad (10)$$

$$\Delta\xi^c = \xi_j^c - \xi_i^c, \Delta\xi^b = \xi_j^b - \xi_i^b, r_i = b - A^b \xi_i^b.$$

(a) *Intersection criterion.*  $\mathcal{Z}_{c,i} \cap \mathcal{Z}_{c,j} \neq \emptyset$  if and only if the following system is feasible:

$$M \Delta \xi^c = N \Delta \xi^b \quad (11a)$$

$$A^c \xi^c = r_i \quad (11b)$$

$$-1 \leq \xi^c \leq 1 \quad (11c)$$

$$-1 \leq \xi^c + \Delta \xi^c \leq 1 \quad (11d)$$

(b) *Linear consistency shortcut.* Let  $L = (I - MM^\dagger)N$  where  $M^\dagger$  is the Moore–Penrose pseudoinverse of  $M$ . Then

$$\exists \Delta \xi^c : M \Delta \xi^c = N \Delta \xi^b \iff L \Delta \xi^b = 0 \quad (12)$$

(c) *Tangent vs. overlap characterization.* Let  $\mathcal{F}$  denote the set of all solutions to (11), and define the strict interior feasible region:

$$\mathcal{F}^\circ = \{(\xi^c, \Delta \xi^c) \in \mathcal{F} \mid |\xi_k^c| < 1, |\xi_k^c + \Delta \xi_k^c| < 1; \forall k\} \quad (13)$$

Then:

$$\begin{aligned} \text{Tangent contact (boundary-only)} &\iff \mathcal{F} \neq \emptyset \text{ and } \mathcal{F}^\circ = \emptyset \\ (14) \end{aligned}$$

$$\text{Interior overlap} \iff \mathcal{F}^\circ \neq \emptyset \quad (15)$$

*Interior overlap implies the intersection contains points in the interior of both leaves, yielding non-zero volume. Tangent contact implies the intersection is confined to boundaries, forming a lower-dimensional face.*

(d) *Adjacency computation.* For any pair of leaves, the adjacency can be determined by:

$$\mathcal{A}_{ij} = \begin{cases} 1 & \text{if } L(\xi_j^b - \xi_i^b) = 0 \text{ and system (11) is feasible} \\ 0 & \text{otherwise} \end{cases} \quad (16)$$

*Proof.* (a) ( $\Rightarrow$ ) Let  $z \in \mathcal{Z}_{c,i} \cap \mathcal{Z}_{c,j}$ . Then there exist  $\xi_i^c, \xi_j^c \in \mathcal{B}_{\infty}^{n_g} = \xi \mid |\xi|_\infty \leq 1$  such that:

$$G^c \xi_i^c + c + G^b \xi_i^b = z \quad (17)$$

$$G^c \xi_j^c + c + G^b \xi_j^b = z \quad (18)$$

$$A^c \xi_i^c + A^b \xi_i^b = b \quad (19)$$

$$A^c \xi_j^c + A^b \xi_j^b = b \quad (20)$$

Setting  $\Delta \xi^c = \xi_j^c - \xi_i^c$  and subtracting yields:

$$G^c \Delta \xi^c = G^b (\xi_j^b - \xi_i^b) = G^b \Delta \xi^b \quad (21)$$

$$A^c \Delta \xi^c = A^b (\xi_j^b - \xi_i^b) = A^b \Delta \xi^b \quad (22)$$

Combined, this gives  $M \Delta \xi^c = N \Delta \xi^b$ . Let  $\xi^c = \xi_i^c$ . Then we have:

$$A^c \xi^c = A^c \xi_i^c = b - A^b \xi_i^b = r_i \quad (23)$$

$$|\xi^c|_\infty = |\xi_i^c|_\infty \leq 1 \quad (24)$$

$$|\xi^c + \Delta \xi^c|_\infty = |\xi_i^c + (\xi_j^c - \xi_i^c)|_\infty = |\xi_j^c|_\infty \leq 1 \quad (25)$$

Thus,  $(\xi^c, \Delta \xi^c)$  satisfies system (11). ( $\Leftarrow$ ) Given  $\xi^c$  and  $\Delta \xi^c$  satisfying (11), define:

$$\xi_i^c = \xi^c \quad (26)$$

$$\xi_j^c = \xi^c - \Delta \xi^c \quad (27)$$

From (11c) and (11d), we have  $\xi_i^c, \xi_j^c \in \mathcal{B}_\infty^{n_g}$ . From (11b),  $A^c \xi_i^c = r_i = b - A^b \xi_i^b$ , thus  $A^c \xi_i^c + A^b \xi_i^b = b$ . From (11a),  $M \Delta \xi^c = N \Delta \xi^b$  implies:

$$A^c(\xi_i^c - \xi_j^c) = A^b(\xi_j^b - \xi_i^b) \quad (28)$$

$$\Rightarrow A^c \xi_j^c + A^b \xi_j^b = A^c \xi_i^c + A^b \xi_i^b = b \quad (29)$$

Define  $z = G^c \xi_i^c + c + G^b \xi_i^b$ . Similarly, from (11a):

$$G^c(\xi_i^c - \xi_j^c) = G^b(\xi_j^b - \xi_i^b) \quad (30)$$

$$\Rightarrow G^c \xi_j^c + G^b \xi_j^b = G^c \xi_i^c + G^b \xi_i^b \quad (31)$$

Thus,  $z = G^c \xi_i^c + c + G^b \xi_i^b \in \mathcal{Z}_{c,i} \cap \mathcal{Z}_{c,j}$ .

(b)  $N \Delta \xi^b$  lies in  $\text{im } M$  if and only if its projection onto  $\text{im } M^\perp$  is zero; this projection is precisely  $(I - M M^\dagger) N \Delta \xi^b = L \Delta \xi^b$ .

(c)  $\mathcal{F}^\circ \neq \emptyset$  means there exists a solution strictly inside both boxes, implying the intersection contains interior points with non-zero volume. When all feasible solutions touch at least one box face ( $|\cdot| = 1$ ), the intersection consists only of boundary points or lower-dimensional faces, resulting in tangent contact.

(d) Adjacency requires both linear consistency ( $L \Delta \xi^b = 0$ ) and feasibility of system (11), which together ensure a non-empty intersection between leaves.  $\square$

**Corollary III.3.** To distinguish between interior overlap and boundary contact of leaves  $\mathcal{Z}_{c,i}$  and  $\mathcal{Z}_{c,j}$ , introduce a slack variable  $\delta \geq 0$  that tightens the box constraints in (11):

$$(11a) \quad (32a)$$

$$(11b) \quad (32b)$$

$$-1 + \delta \leq \xi^c \leq 1 - \delta \quad (32c)$$

$$-1 + \delta \leq \xi^c + \Delta \xi^c \leq 1 - \delta \quad (32d)$$

Consider the linear program

$$\delta^* = \max_{\xi^c, \Delta \xi^c, \delta} ; \delta \quad \text{s.t. (32)} \quad (33)$$

Then:

- $\delta^* > 0 \iff$  interior overlap (intersection contains interior points)
- $\delta^* = 0 \iff$  boundary contact (intersection confined to boundaries)

Intuitively,  $\delta^*$  quantifies the maximal uniform contraction of the box constraints that preserves feasibility.

**Corollary III.4.** For any two adjacent leaf nodes  $\mathcal{Z}_{c,i}$  and  $\mathcal{Z}_{c,j}$  with  $\mathcal{A}_{ij} = 1$ , their shared face can be computed as a generalized intersection of constrained zonotopes [14]. Given  $\mathcal{Z}_{c,i} = \langle G^c, c + G^b \xi_i^b, A^c, b - A^b \xi_i^b \rangle$  and  $\mathcal{Z}_{c,j} = \langle G^c, c + G^b \xi_j^b, A^c, b - A^b \xi_j^b \rangle$ , their shared face is:

$$\mathcal{F}_{ij} = \mathcal{Z}_{c,i} \cap_{\mathbf{I}} \mathcal{Z}_{c,j} = \left\{ [G^c \mathbf{0}], c + G^b \xi_i^b, \begin{bmatrix} A^c & \mathbf{0} \\ \mathbf{0} & A^c \\ G^c & -G^c \end{bmatrix}, \begin{bmatrix} b - A^b \xi_i^b \\ b - A^b \xi_j^b \\ G^b(\xi_j^b - \xi_i^b) \end{bmatrix} \right\} \quad (34)$$

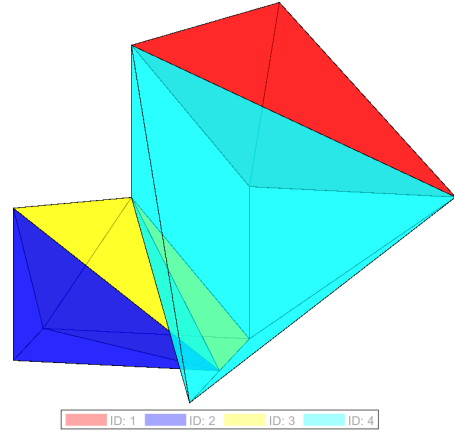


Fig. 3: Hybrid zonotope with four leaf nodes (1-4) and their adjacency.

where  $\mathbf{I}$  is the identity matrix.

Furthermore, the shared face  $\mathcal{F}_{ij}$  is a constrained zonotope of dimension at most  $(n - 1)$  with non-zero  $(n - 1)$ -dimensional Hausdorff measure. This follows from the fact that the constraint  $G^c \xi = G^b(\xi_j^b - \xi_i^b)$  imposes at least one linear constraint on  $\xi$ , reducing the dimension by at least 1. Since  $\xi_i^b \neq \xi_j^b$  for adjacent leaves (they are distinct), the constraint is non-trivial and  $\mathcal{F}_{ij}$  has positive  $(n - 1)$ -dimensional measure.

This computation of shared faces is based on the generalized intersection operation for constrained zonotopes as established in [14]. The dimension reduction property is critical for our sampling-based motion planning approach: by focusing samples on these  $(n - 1)$ -dimensional shared faces rather than  $n$ -dimensional volumes, we effectively reduce the dimensionality of the search space while ensuring connectivity between adjacent regions of the free space.

**Example 2.** Consider a hybrid zonotope  $\mathcal{Z}_h = \langle G^c, G^b, c, A^c, A^b, b \rangle$  in  $\mathbb{R}^3$  that decomposes a workspace into four distinct leaf nodes representing convex regions of the free space. Figure 3 shows the geometric representation of these leaf nodes.

The adjacency matrix  $\mathcal{A}$  for this configuration is:

ID	1	2	3	4
1	0	0	0	1
2	0	0	1	0
3	0	1	0	1
4	1	0	1	0

(35)

This adjacency matrix indicates that leaf node 1 is adjacent to leaf node 4, leaf node 4 is adjacent to leaf node 3, and leaf node 2 is adjacent to leaf node 3, the only possible route is  $1 \rightarrow 4 \rightarrow 3 \rightarrow 2$ . For any pair of adjacent leaf nodes, we can compute their shared face using Corollary III.4. For example, the shared face between leaf nodes 1 and 4 is obtained by:

$$\mathcal{F}_{1,4} = \mathcal{Z}_{c,1} \cap_{\mathbf{I}} \mathcal{Z}_{c,4} \quad (36)$$

Our algorithm generates samples on the shared faces

$\mathcal{F}_{1,4}$ ,  $\mathcal{F}_{4,3}$ , and  $\mathcal{F}_{3,2}$  to optimize the path through these waypoints, achieving dimension reduction by sampling on lower-dimensional interfaces rather than the full 3D space.

The adjacency matrix  $\mathcal{A}$  and shared face computations from III.4 provide the topological foundation for our planning algorithm. We now present how this structure enables efficient path optimization through informed sampling and iterative refinement.

#### D. Informed sampling and ellipsotope refinement

With the adjacency structure established, we employ an iterative refinement process that alternates between path optimization and reachable set updates, as depicted in Figure 1(c)-(e). This section presents our sampling strategy on shared faces and the ellipsotope-based pruning mechanism.

1) *Sampling on shared faces:* Rather than sampling uniformly throughout the  $n$ -dimensional state space, we exploit the structure revealed in III.2 to focus samples on  $(n - 1)$ -dimensional shared faces  $\mathcal{F}_{ij}$  between adjacent leaves. For a path  $p = (i_0, i_1, \dots, i_k)$  through the adjacency graph, we generate waypoint samples  $s = (s_1, \dots, s_{k-1})$  where each  $s_j \in \mathcal{F}_{i_j, i_{j+1}}$ .

The path cost for a given set of waypoints is:

$$c(\sigma_s) = \|x_{\text{start}} - s_1\|_2 + \sum_{j=1}^{k-2} \|s_j - s_{j+1}\|_2 + \|s_{k-1} - x_{\text{goal}}\|_2 \quad (37)$$

The convexity of leaf nodes guarantees that straight-line segments between consecutive waypoints remain collision-free, enabling efficient local optimization within this reduced-dimensional space.

2) *Ellipsotope-based reachable set refinement:* As illustrated in Figure 1(d)-(e), each discovered path with cost  $c_{\text{best}}$  induces an ellipsotope that bounds all potentially improving solutions:

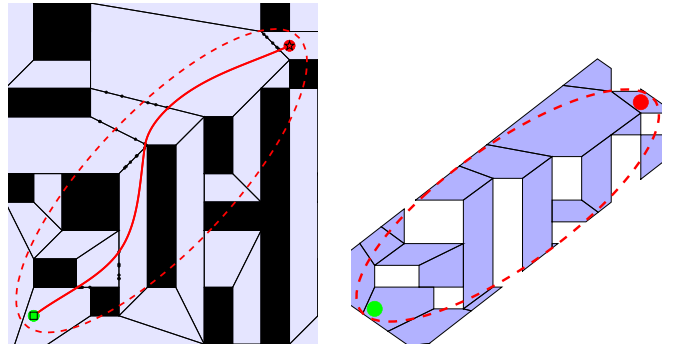
$$\mathcal{E} = \{x \in \mathbb{R}^n : \|x - x_{\text{start}}\|_2 + \|x - x_{\text{goal}}\|_2 \leq c_{\text{best}}\} \quad (38)$$

This ellipsotope, shown as the dashed ellipse in Figure 1(d), enables systematic pruning of the search space. The intersection  $\mathcal{E} \cap \mathcal{Z}_h$  yields the refined reachable set depicted in Figure 1(e), focusing subsequent iterations on regions that can potentially improve the solution.

Algorithm 1 implements the complete HZ-MP pipeline illustrated in Figure 1. The algorithm proceeds through three main phases: decomposition and adjacency computation (lines 1-7, corresponding to Figure 1(a)-(c)), parallel path optimization (lines 12-20), and ellipsotope-based refinement (lines 17-18, corresponding to Figure 1(d)-(e)).

The updateReachableSet function (Algorithm 2) constructs the ellipsotope based on the current best path cost and updates the adjacency relationships to reflect the pruned search space. This iterative refinement ensures that computational resources are focused on regions with potential for improvement, accelerating convergence to the optimal solution.

By combining hybrid zonotope decomposition, dimension-reduced sampling on shared faces, and ellipsotope-based



(a) Green dot is start, red dot is target, red curve is the current shortest path. The red dashed ellipse shows ellipsotope corresponding to the past cost values.  
(b) Intersection between hybrid zonotope and constrained zonotope (from ellipsotope) to update the feasible space for next motion planning iteration.

Fig. 4: Illustration of ellipsotope-informed sampling with path cost.

pruning, HZ-MP achieves an effective balance between exploration efficiency and solution quality. The parallel processing of multiple paths ensures rapid discovery of initial solutions, while the iterative refinement guarantees asymptotic convergence to the global optimum.

Algorithm 1 operates in three phases. First, it constructs the hybrid zonotope decomposition and identifies leaves containing start and goal states through membership queries:

$$i_{\text{start}} = \arg \min_{i \in \{1, \dots, m\}} \{i : x_{\text{start}} \in \mathcal{Z}_i\}$$

$$i_{\text{goal}} = \arg \min_{i \in \{1, \dots, m\}} \{i : x_{\text{goal}} \in \mathcal{Z}_i\}$$

The algorithm then enumerates all feasible paths  $\mathcal{P}$  between these leaves using breadth-first search on the adjacency graph  $\mathcal{A}$ .

The core optimization phase (lines 12-20) explores each path  $p = (i_0, i_1, \dots, i_k) \in \mathcal{P}$  in parallel. For each path, the algorithm generates samples  $S_p = \{s_j^{(l)} : s_j^{(l)} \sim \text{Uniform}(\mathcal{F}_{i_j, i_{j+1}}), l = 1, \dots, N_s\}$  on the shared faces between consecutive leaves. These samples define waypoints for potential solution paths, and the algorithm solves the discrete optimization problem  $s_p^* = \arg \min_{s \in S_p} c(\sigma_s)$  to find the best configuration for each path. The final phase (lines 17-18) updates the reachable ellipsoid based on the current best solution and prunes paths that cannot improve upon it.

3) *Path Cost Structure:* For a path defined by waypoints  $s = (s_1, \dots, s_{k-1})$  where each  $s_j \in \mathcal{F}_{i_j, i_{j+1}}$ , the total cost is computed as:

$$c(\sigma_s) = \|x_{\text{start}} - s_1\|_2 + \sum_{j=1}^{k-2} \|s_j - s_{j+1}\|_2 + \|s_{k-1} - x_{\text{goal}}\|_2 \quad (39)$$

Since each leaf node is convex, the straight-line segments between consecutive waypoints are guaranteed to be collision-free, eliminating the need for explicit collision checking during path evaluation.

---

**Algorithm 1** Informed Hybrid Zonotope Motion Planning (HZ-MP)

---

**Input:** Start state  $x_{\text{start}}$ , goal point  $x_{\text{goal}}$ , state space  $\mathcal{X}$ , obstacles  $\mathcal{X}_{\text{obs}}$ , max iterations  $N_{\text{max}}$

**Output:** Optimal path solution  $\sigma^*$

- 1:  $\mathcal{Z}_h = \text{FreeSpaceDecomposition}(\mathcal{X}, \mathcal{X}_{\text{obs}})$  ▷ III-B
- 2:  $\mathcal{L} = \text{LeafNodes}(\mathcal{Z}_h)$
- 3:  $\mathcal{A} = \text{AdjacencyMatrix}(\mathcal{Z}_h, \mathcal{L})$  ▷ III.2
- 4:  $i_{\text{start}} = \text{findContainingLeaf}(x_{\text{start}}, \mathcal{L})$
- 5:  $i_{\text{goal}} = \text{findContainingLeaf}(x_{\text{goal}}, \mathcal{L})$
- 6:  $\mathcal{P} = \text{findAllConnectedPaths}(i_{\text{start}}, i_{\text{goal}}, \mathcal{A})$
- 7:  $\mathcal{F} = \text{computeSharedFaces}(\mathcal{L}, \mathcal{A})$  ▷ III.4
- 8:  $c_{\text{best}} = \infty$
- 9:  $\sigma^* = \emptyset$
- 10:  $iter = 0$
- 11: Initialize parallel search processes
- 12: **while**  $iter < N_{\text{max}}$  and !converged **do**
- 13:   **for** each path  $p \in \mathcal{P}$  **in parallel do**
- 14:      $S_p = \text{generateSamples}(\mathcal{F}, p)$
- 15:      $c_p, \sigma_p = \text{optimizePath}(x_{\text{start}}, x_{\text{goal}}, S_p, \mathcal{L})$
- 16:     **if**  $c_p < c_{\text{best}}$  **then**
- 17:        $\text{updateGlobalBest}(c_p, \sigma_p)$
- 18:        $\mathcal{E} = \text{updateReachableSet}(x_{\text{start}}, x_{\text{goal}}, c_p)$
- 19:     **end if**
- 20:   **end for**
- 21:    $iter = iter + 1$
- 22: **end while**
- 23: **return**  $\sigma^*$

---

4) *Sampling Methods:* Uniform sampling on  $(n - 1)$ -dimensional faces requires specialized techniques. The Hit-and-Run algorithm [15] generates samples by iteratively updating a current point  $x^{(t)} \in \mathcal{F}_{ij}$ . At each iteration, it samples a random direction  $d \sim \mathcal{N}(0, P_{\mathcal{F}_{ij}})$  where  $P_{\mathcal{F}_{ij}}$  projects onto the face tangent space, computes the feasible interval  $\Lambda = \{\lambda : x^{(t)} + \lambda d \in \mathcal{F}_{ij}\}$  via linear programming, and updates the position as  $x^{(t+1)} = x^{(t)} + \lambda d$  where  $\lambda \sim \text{Uniform}(\Lambda)$ . For faces with complex geometry, we alternatively employ the Billiard Walk method [16], which simulates Hamiltonian dynamics with specular reflections at boundaries to ensure ergodic exploration.

#### E. Ellipsotope-informed path refinement

Upon discovering a path with cost  $c_{\text{best}}$ , the algorithm constructs an ellipsotope representing the reachable set:

$$\mathcal{E} = \{x \in \mathbb{R}^n : \|x - x_{\text{start}}\|_2 + \|x - x_{\text{goal}}\|_2 \leq c_{\text{best}}\} \quad (40)$$

This can be expressed as an ellipsotope (Definition II.3) with  $p = 2$  and  $\mathcal{I} = \{\{1, \dots, n_g\}\}$ :

$$\mathcal{E} = \mathcal{E}_2(c, G) = \{c + G\xi : \|\xi\|_2 \leq 1\} \quad (41)$$

where the center  $c = \frac{1}{2}(x_{\text{start}} + x_{\text{goal}})$  and the generator matrix  $G \in \mathbb{R}^{n \times n}$  is constructed such that the ellipsotope has semi-major axis  $a = c_{\text{best}}/2$  along the direction  $\hat{d} = \frac{x_{\text{goal}} - x_{\text{start}}}{\|x_{\text{goal}} - x_{\text{start}}\|_2}$  and semi-minor axes  $b = \sqrt{a^2 - \|d\|^2/4}$  in the orthogonal directions.

---

**Algorithm 2** Update Reachable Set with Ellipsotope

---

**Input:** Start point  $x_{\text{start}}$ , goal point  $x_{\text{goal}}$ , current best cost  $c_{\text{best}}$

**Output:** Updated ellipsotope  $\mathcal{E}$  representing reachable set

- 1:  $d = x_{\text{goal}} - x_{\text{start}}$
- 2:  $\|d\| = \sqrt{d^T d}$
- 3:  $\hat{d} = d/\|d\|$
- 4:  $c = (x_{\text{start}} + x_{\text{goal}})/2$
- 5:  $a = c_{\text{best}}/2$
- 6:  $b = \sqrt{a^2 - (\|d\|/2)^2}$
- 7:  $Q = \text{constructShapeMatrix}(\hat{d}, a, b)$
- 8:  $\mathcal{E} = \mathcal{E}_2(c, Q)$  ▷ II.3
- 9:  $\mathcal{A} = \text{updateLeafAdjacency}(\mathcal{L}, \mathcal{E})$
- 10:  $\mathcal{P} = \text{updateConnectedPaths}(i_{\text{start}}, i_{\text{goal}}, \mathcal{A})$
- 11: **return**  $\mathcal{E}$

---

The ellipsotope representation precisely bounds all states that could potentially improve the current solution while enabling efficient intersection operations with constrained zonotope leaves. The intersection between an ellipsotope and a constrained zonotope can be computed using constrained convex generators[17], which provides a systematic method for combining their constraints, as illustrated in Figure 4a. The algorithm classifies leaf nodes based on their intersection with  $\mathcal{E}$ : Inactive:  $\mathcal{Z}_{c,i} \cap \mathcal{E} = \emptyset$ ; Partial:  $\emptyset \neq \mathcal{Z}_{c,i} \cap \mathcal{E} \neq \mathcal{Z}_{c,i}$ ; Active:  $\mathcal{Z}_{c,i} \subseteq \mathcal{E}$ . The intersection  $\mathcal{Z}_{c,i} \cap \mathcal{E}$  can be computed using the techniques from [18], enabling rapid pruning of infeasible regions. However, to further simplify computation, we can also convert ellipsotopes to constrained zonotope representation, as illustrated in Figure 4b. This conversion allows us to perform all set operations within the zonotope-based framework, maintaining computational efficiency.

*Theoretical Guarantees:* The hybrid zonotope framework transforms motion planning in obstacle-cluttered environments into convex subproblems, enabling strong theoretical guarantees.

**Theorem III.5** (Probabilistic Completeness). *Let  $\mathcal{Z}_h = \langle G^c, G^b, c, A^c, A^b, b \rangle$  be a hybrid zonotope representation of  $\mathcal{X}_{\text{free}}$ . If a feasible solution exists, then  $\lim_{N_s \rightarrow \infty} \mathbb{P}[\text{solution found}] = 1$  where  $N_s$  is the number of samples per shared face.*

*Proof.* Let  $\sigma^* : [0, 1] \rightarrow \mathcal{X}_{\text{free}}$  be a feasible path. Since  $\mathcal{Z}_h$  represents  $\mathcal{X}_{\text{free}}$ , there exists a sequence of binary factors  $\{\xi_t^{b,*}\}_{t \in [0,1]}$  such that:

$$\sigma^*(t) = G^c \xi_t^{c,*} + G^b \xi_t^{b,*} + c$$

for some continuous factors  $\xi_t^{c,*} \in \mathcal{B}_{\infty}^{n_g}$  satisfying  $A^c \xi_t^{c,*} + A^b \xi_t^{b,*} = b$ .

Since  $\xi_t^{b,*} \in \{-1, 1\}^{n_b}$  is discrete and the path is continuous, there exist times  $0 = t_0 < t_1 < \dots < t_k = 1$  where  $\xi_{t_j}^{b,*} \neq \xi_{t_{j+1}}^{b,*}$ . This defines a sequence of leaves  $\mathcal{I}^* = (i_0, \dots, i_k)$  with transition points  $s_j^* = \sigma^*(t_j) \in \mathcal{F}_{i_j, i_{j+1}}$ .

By Corollary III.4, each  $\mathcal{F}_{i_j, i_{j+1}}$  has positive  $(n - 1)$ -dimensional measure  $\mu_{n-1}(\mathcal{F}_{i_j, i_{j+1}}) > 0$ . For uniform

sampling on  $\mathcal{F}_{i_j, i_{j+1}}$ :

$$\mathbb{P}[\|s_j^{(l)} - s_j^*\| < \epsilon] \geq \frac{\mu_{n-1}(B_\epsilon(s_j^*) \cap \mathcal{F}_{i_j, i_{j+1}})}{\mu_{n-1}(\mathcal{F}_{i_j, i_{j+1}})} =: p_\epsilon > 0$$

Therefore:

$$\mathbb{P}\left[\min_{l \in \{1, \dots, N_s\}} \|s_j^{(l)} - s_j^*\| < \epsilon\right] = 1 - (1 - p_\epsilon)^{N_s} \rightarrow 1 \text{ as } N_s \rightarrow \infty$$

Since each leaf  $\mathcal{Z}_{c,i}$  is convex (being a constrained zonotope), straight-line paths between points within a leaf are collision-free. Thus, the algorithm finds a feasible path with probability approaching 1.  $\square$

**Theorem III.6** (Asymptotic Optimality). *Under uniform sampling on shared faces of  $\mathcal{Z}_h$ :  $\lim_{N_s \rightarrow \infty} \mathbb{E}[c_{best}] = c^*$  where  $c^*$  is the optimal cost.*

*Proof.* The optimal path  $\sigma^*$  with cost  $c^*$  passes through transition points  $\mathbf{s}^* = (s_1^*, \dots, s_{k-1}^*)$ . The cost function for waypoints  $\mathbf{s} = (s_1, \dots, s_{k-1})$  is:

$$c(\sigma_{\mathbf{s}}) = \|x_{start} - s_1\|_2 + \sum_{j=1}^{k-2} \|s_j - s_{j+1}\|_2 + \|s_{k-1} - x_{goal}\|_2$$

This function is Lipschitz continuous with constant  $L = 2\sqrt{k}$  since:

$$|c(\sigma_{\mathbf{s}}) - c(\sigma'_{\mathbf{s}'})| \leq \sum_{j=0}^k \|s_j - s'_j\|_2 \leq 2\sqrt{k}\|\mathbf{s} - \mathbf{s}'\|_\infty$$

where we define  $s_0 = x_{start}$  and  $s_k = x_{goal}$ .

By uniform sampling on each constrained zonotope face  $\mathcal{F}_{i_j, i_{j+1}}$  and the strong law of large numbers for empirical measures on compact sets:

$$\delta_N := \max_{j \in \{1, \dots, k-1\}} \min_{l \in \{1, \dots, N_s\}} \|s_j^{(l)} - s_j^*\|_2 \rightarrow 0 \text{ a.s.}$$

By Lipschitz continuity:  $|c_{best} - c^*| \leq L\delta_N \rightarrow 0$  a.s., yielding  $\lim_{N_s \rightarrow \infty} \mathbb{E}[c_{best}] = c^*$ .  $\square$

#### IV. NUMERICAL EXAMPLES

We evaluate the proposed hybrid zonotope-based motion planning algorithm on challenging scenarios that demonstrate its effectiveness in complex environments with narrow passages.

##### A. Convergence analysis

We evaluate our algorithm on a planar maze environment  $\mathcal{X} = [-100, 800] \times [-100, 600]$  containing 13 obstacles: rectangular barriers, polygonal approximations of circles, U-shaped regions, star polygons, and narrow passages (60 cm width). The start state is  $x_{start} = (400, 250)^T$  and goal state is  $x_{goal} = (385, 470)^T$ , requiring navigation through the maze structure and around multiple obstacles. This environment exemplifies the challenges of motion planning in cluttered spaces with both narrow passages and complex obstacle geometries.

Figures 5 demonstrate the algorithm's convergence behavior in a complex 2D environment. The algorithm executed 8 iterations, with significant solution improvements occurring

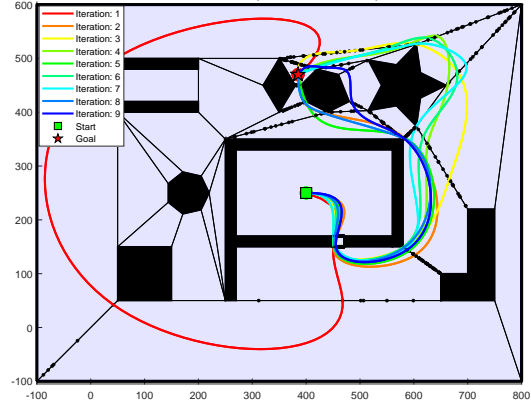


Fig. 5: Motion planning scenario showing the environment with obstacles (gray regions), the start point (green), the goal region (red), and the solution path found by our algorithm. The map coordinates are given in centimeters.

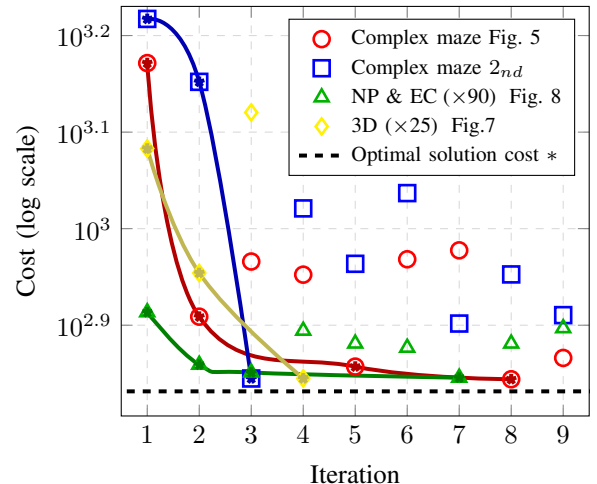


Fig. 6: Convergence analysis across different environments showing the stochastic nature of our sampling-based approach. Markers indicate costs at each iteration, while stars connected by smooth curves represent iterations where a better solution was found and adopted as the new best. The non-monotonic behavior between starred points reflects the exploration-exploitation trade-off inherent in sampling-based methods.

at iterations 1, 2, 5, and 8 (marked with green stars). The final optimal solution achieved a cost of 698.603. The cost function exhibits rapid initial decrease followed by stabilization, validating our theoretical convergence guarantees. The hybrid zonotope decomposition enables systematic exploration of multiple homotopy classes, efficiently identifying the globally optimal path.

##### B. 3D narrow passage navigation

We evaluate the algorithm in a three-dimensional environment  $\mathcal{X} = [-15, 15] \times [0, 15] \times [0, 5] \subset \mathbb{R}^3$ . The environment features a central wall at  $(0, 0, 2.5)^T$  spanning 13 m vertically with a critical narrow passage of 1 m height at  $z = 4.5$

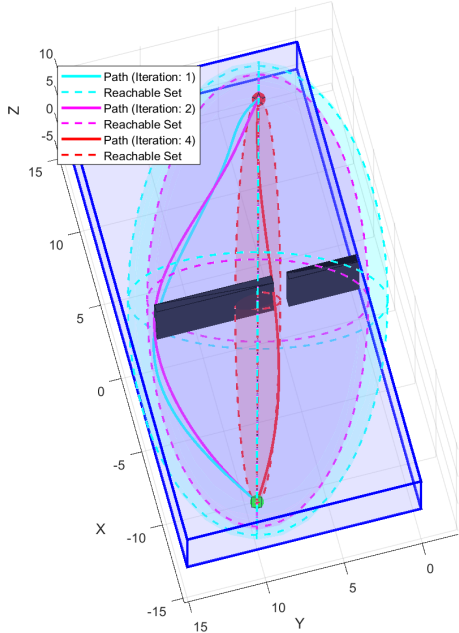


Fig. 7: 3D narrow passage scenario showing the evolution of paths and reachable sets across multiple iterations. The blue box represents the environment boundaries, the black region is an obstacle creating a narrow passage, the green cube is the start position, and the red sphere is the goal. Different colored paths and ellipsoidal reachable sets correspond to different iterations.

m. All walls have thickness 0.3 m, creating a challenging topology where the optimal path must navigate through aligned openings. The start state is  $x_{\text{start}} = (-13, 10, 3)^T$  and goal state is  $x_{\text{goal}} = (13, 3, 2)^T$ , requiring navigation through the narrow gap, demonstrating the algorithm’s capability in constrained 3D spaces.

Figure 7 illustrates the algorithm’s iterative refinement process. The cyan path (iteration 1) takes a conservative route with a large reachable ellipsoid, the magenta path (iteration 2) improves with a reduced reachable set, and the red path (iteration 4) identifies the optimal trajectory through the narrow passage. The progressively shrinking ellipsoidal reachable sets demonstrate the effectiveness of our informed sampling strategy, concentrating computational effort in promising regions while maintaining completeness guarantees.

### C. Narrow passages and enclosure example

We further evaluate our algorithm on a planar enclosure environment  $\mathcal{X} = [0, 10] \times [0, 10] \subset \mathbb{R}^2$  featuring a rectangular enclosure with interior dimensions approximately  $6 \times 4$  units centered at  $(5, 4)^T$ . The enclosure walls have thickness 0.3 units and contain a critical narrow opening of width 0.8 units on the left wall at height  $y = 4$ . The start state  $x_{\text{start}} = (3, 3)^T$  is positioned outside the enclosure, while the goal state  $x_{\text{goal}} = (7, 5)^T$  lies within the enclosed region, necessitating passage through the narrow opening. This configuration exemplifies the narrow passage problem

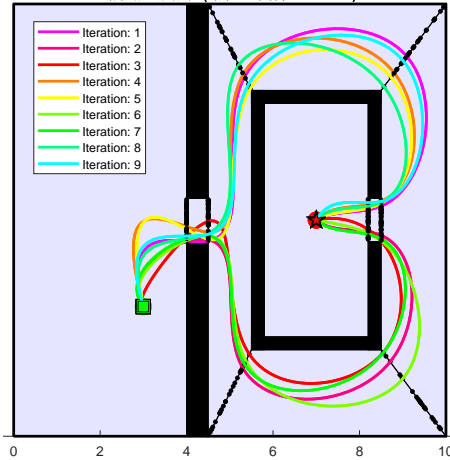


Fig. 8: Narrow passage and enclosure scenario showing the hybrid zonotope decomposition. The numbered regions (0, 1, 2) represent different leaf nodes, with region 012 indicating the critical shared face at the narrow passage. The algorithm successfully identifies and navigates through this constrained opening.

where the measure of the feasible region connecting start to goal is vanishingly small relative to the total free space volume.

Figure 8 demonstrates the algorithm’s capability in extremely constrained environments. The hybrid zonotope decomposition explicitly captures the narrow passage as a shared face between leaf nodes, ensuring high sampling density precisely where needed. By sampling on  $(n - 1)$ -dimensional shared faces rather than  $n$ -dimensional volumes, our approach maintains computational efficiency while guaranteeing discovery of feasible paths through narrow openings. The explicit topological representation ensures these critical regions are systematically explored, addressing a fundamental challenge in sampling-based motion planning.

These results confirm that the hybrid zonotope framework effectively addresses the narrow passage problem—a fundamental challenge in motion planning—through dimension reduction and topology-aware sampling.

## V. CONCLUSION

We presented a motion planning algorithm that leverages hybrid zonotope decomposition to transform complex planning problems into sequences of convex subproblems. The key innovation—sampling on  $(n - 1)$ -dimensional shared faces rather than  $n$ -dimensional volumes—directly addresses the narrow passage problem while maintaining theoretical guarantees of probabilistic completeness and asymptotic optimality.

Our approach achieves local linear convergence within convex regions and demonstrates rapid global convergence through ellipsotope-informed refinement. Experimental results confirm the algorithm’s effectiveness across diverse environments, from 2D mazes to 3D narrow passages. While the initial decomposition incurs computational cost, this

amortizes over multiple queries in static environments.

Future work includes extending the framework to dynamic environments and kinodynamic constraints. By unifying geometric decomposition with sampling-based planning, this work provides a principled solution to motion planning in complex, constrained spaces.

## REFERENCES

- [1] D. Ioan, I. Prodan, S. Olaru, F. Stoican, and S. I. Niculescu, “Mixed-integer programming in motion planning,” *Annual Reviews in Control*, vol. 51, pp. 65–87, 2021.
- [2] T. J. Bird, H. C. Pangborn, N. Jain, and J. P. Koeln, “Hybrid zonotopes: A new set representation for reachability analysis of mixed logical dynamical systems,” *Automatica*, vol. 154, p. 111107, 2023.
- [3] J. A. Robbins, S. B. Brennan, and H. C. Pangborn, “Efficient solution of mixed-integer MPC problems for obstacle avoidance using hybrid zonotopes,” in *Proc. 63rd IEEE Conf. on Decision and Control (CDC)*, 2024, pp. 8199–8206.
- [4] S. Shoja, D. Arnström, and D. Axehill, “Overall complexity certification of a standard branch and bound method for mixed-integer quadratic programming,” in *2022 American Control Conference (ACC)*. IEEE, 2022, pp. 4957–4964.
- [5] L. E. Kavraki, P. Švestka, J.-C. Latombe, and M. H. Overmars, “Probabilistic roadmaps for path planning in high-dimensional configuration spaces,” *IEEE Transactions on Robotics and Automation*, vol. 12, no. 4, pp. 566–580, 1996.
- [6] S. Karaman and E. Frazzoli, “Sampling-based algorithms for optimal motion planning,” in *Robotics: Science and Systems*, 2011.
- [7] J. D. Gammell, S. S. Srinivasa, and T. D. Barfoot, “Informed rrt\*: Optimal sampling-based path planning focused via direct sampling of an admissible ellipsoidal heuristic,” in *IEEE/RSJ International Conference on Intelligent Robots and Systems*. IEEE, 2014, pp. 2997–3004.
- [8] M. P. Strub and J. D. Gammell, “Adaptively informed trees (AIT\*) and effort informed trees (EIT\*): Asymmetric bidirectional sampling-based path planning,” *Int. Journal of Robotics Research*, vol. 41, no. 4, pp. 390–417, 2022.
- [9] S. Kousik, A. Dai, and G. X. Gao, “Ellipsotopes: Uniting ellipsoids and zonotopes for reachability analysis and fault detection,” *IEEE Transactions on Automatic Control*, vol. 68, no. 6, pp. 3440–3452, 2023.
- [10] P. Hachenberger, L. Kettner, and K. Mehlhorn, “Boolean operations on 3D selective Nef complexes: Data structure, algorithms, optimized implementation and experiments,” *Computational Geometry*, vol. 38, no. 1-2, pp. 64–99, 2007.
- [11] The CGAL Project, *CGAL User and Reference Manual*, 6.0.1 ed. CGAL Editorial Board, 2024. [Online]. Available: <https://doc.cgal.org/6.0.1/Manual/packages.html>
- [12] J. A. Robbins, J. A. Siefert, S. Brennan, and H. C. Pangborn, “Mixed-integer mpc-based motion planning using hybrid zonotopes with tight relaxations,” *arXiv preprint arXiv:2411.01286*, 2024.
- [13] J. Koeln, T. J. Bird, J. Siefert, J. Ruths, H. C. Pangborn, and N. Jain, “zonolab: A matlab toolbox for set-based control systems analysis using hybrid zonotopes,” in *2024 American Control Conference (ACC)*. IEEE, 2024, pp. 2513–2520.
- [14] J. K. Scott, D. M. Raimondo, G. R. Marseglia, and R. D. Braatz, “Constrained zonotopes: A new tool for set-based estimation and fault detection,” *Automatica*, vol. 69, pp. 126–136, 2016.
- [15] R. L. Smith, “Efficient monte carlo procedures for generating points uniformly distributed over bounded regions,” *Operations Research*, vol. 32, no. 6, pp. 1296–1308, 1984.
- [16] B. T. Polyak and E. N. Gryazina, “Billiard walk - a new sampling algorithm for control and optimization,” in *19th IFAC World Congress*, 2014, pp. 6123–6128.
- [17] D. Silvestre, “Constrained convex generators: A tool suitable for set-based estimation with range and bearing measurements,” *IEEE Control Systems Letters*, vol. 6, pp. 1610–1615, 2022.
- [18] A. Kulmburg, I. Brkan, and M. Althoff, “Search-based and stochastic solutions to the zonotope and ellipsotope containment problems,” in *2024 European Control Conference (ECC)*, 2024, pp. 1057–1064.